Flux difference splitting for the Euler equations with axial symmetry*

P. GLAISTER

Department of Mathematics, University of Reading, P.O. Box 220, Whiteknights, Reading, Berkshire RG6 2AX, United Kingdom

Abstract. An approximate (linearised) Riemann solver is presented for the solution of the Euler equations of gas dynamics for axially symmetric flows. The method is Roe's flux difference splitting with a technique for dealing with source terms and incorporates operator splitting. Results for the problem of a converging spherical shock are presented.

1. Introduction

The (linearised) approximate Riemann solver of Roe [1] and extensions given by Glaister [2] have been highly successful in applications to problems governed by the "one-dimensional" Euler equations with slab, cylindrical or spherical symmetry. In the present paper we seek to extend these techniques to the "two-dimensional" Euler equations with axial symmetry, incorporating the technique of operator splitting. The resulting scheme is applied to a strongly shocked axially symmetric flow.

In Sec. 2 we give the differential equations for the axially symmetric flow of an inviscid perfect gas and describe the details of the flux difference splitting scheme for the approximate solution of these equations. In Sec. 3 we describe a test problem with axial symmetry and display the numerical results achieved for this problem using the scheme of Sec. 2.

2. Flux difference splitting

In this section we consider a finite difference approximation for the solution of the Euler equations of gas dynamics with axial symmetry.

The Euler equations governing axially symmetric flow of a compressible inviscid fluid may be written in the form

$$
\begin{pmatrix} \varrho \\ \varrho u \\ \varrho v \\ e \end{pmatrix}_t + \frac{1}{R} \begin{pmatrix} R\varrho u \\ R\varrho u^2 \\ R\varrho uv \\ Ru(e+p) \end{pmatrix}_R + \begin{pmatrix} \varrho v \\ \varrho uv \\ \varrho v^2 \\ v(e+p) \end{pmatrix}_z = \begin{pmatrix} 0 \\ -p_R \\ -p_z \\ 0 \end{pmatrix} \tag{2.1}
$$

and

$$e = \frac{p}{\gamma - 1} + \tfrac{1}{2}\varrho(u^2 + v^2),\tag{2.2}$$

where $\varrho = \varrho(R, z, t)$, $u = u(R, z, t)$, $v = v(R, z, t)$, $p = p(R, z, t)$ and $e = e(R, z, t)$ represent the density, velocity in the R, z coordinate directions, pressure and total energy, respectively, at a general position (R, z) and time t. The radial coordinate R is given by $R = \sqrt{x^2 + y^2}$ where (x, y, z) are Cartesian coordinates. The fluid is assumed to be ideal with a ratio of specific heat capacities γ.

We begin by rewriting equations (2.1) in the form

$$(Rw)_t + \big(Rf(w)\big)_R + \big(Rg(w)\big)_z = r(w)\tag{2.3}$$

where

$$w = (\varrho, \varrho u, \varrho v, e)^T,\tag{2.4a}$$

$$f(w) = \big(\varrho u, p + \varrho u^2, \varrho uv, u(e + p)\big)^T,\tag{2.4b}$$

$$g(w) = \big(\varrho v, \varrho uv, p + \varrho v^2, v(e + p)\big)^T\tag{2.4c}$$

and

$$r(w) = \left(0, p \frac{\partial}{\partial R}(R), 0, 0\right)^T.\tag{2.4d}$$

(N.B. The reason that we leave the term $p(\partial/\partial R)(R)$ in equation (2.4d) will become apparent later.)

If we define a new variable $W = Rw$ and notice that $Rf(w) = f(Rw) = F(W)$, then equation (2.3) can be written as

$$W_t + F(W)_R + G(W)_z = r(w)\tag{2.5}$$

where

$$W = (\mathscr{R}, \mathscr{R}U, \mathscr{R}V, E)^T,\tag{2.6a}$$

$$F(W) = \big(\mathscr{R}U, P + \mathscr{R}U^2, \mathscr{R}UV, U(E + P)\big)^T,\tag{2.6b}$$

$$G(W) = \big(\mathscr{R}V, \mathscr{R}UV, P + \mathscr{R}V^2, V(E + P)\big)^T,\tag{2.6c}$$

$$r(w) = \left(0, p \frac{\partial}{\partial R}(R), 0, 0\right)^T\tag{2.6d}$$

and

$$E = \frac{P}{\gamma - 1} + \tfrac{1}{2}\mathcal{R}(U^2 + V^2).$$ (2.6e)

This gives rise to new "conserved" variables $\mathcal{R}$, M, N, E where $\mathcal{R} = R\varrho$, $M = Rm$, $N = Rn$ and $E = Re$. (Here m, n denote the components of the momentum in the increasing R- and z-directions, respectively.) It also gives a new "pressure" variable $P = Rp$. Quantities with dimension of velocity are unaltered, e.g., the components of velocity $u = U$, $v = V$, sound speed $a = \sqrt{\gamma p/\varrho} = \sqrt{\gamma P/\mathcal{R}}$ and enthalpy $h = (e + p)/\varrho = (E + P)/\mathcal{R} = H$. In particular the matrices $A = \partial F(W)/\partial W$, $B = \partial G(W)/\partial W$ involve only velocities and are the same as $\partial f(w)/\partial w$, $\partial g(w)/\partial w$, respectively.

We now consider solving equations (2.5)–(2.6e) using the technique of operator splitting. In particular, we propose solving

$$W_t + F(W)_R = r(w)$$ (2.7)

on an R-coordinate line, $z = z_0$, and solving

$$W_t + G(W)_z = 0$$ (2.8)

on a z-coordinate line, $R = R_0$. (We have associated the term $r(w)$ with (2.7) because the only non-zero component $p(\partial/\partial R)(R)$ represents a change in the direction R increasing.) We now propose a finite difference algorithm for the solution of equations (2.7) or (2.8) by noticing the similarity to the Cartesian case (i.e., equation (2.8) with $R = $ constant).

We begin by considering equation (2.7). Consider a fixed grid in space and time with grid sizes ΔR, Δt, respectively, and label the points on an R-coordinate line so that $R_j = R_{j-1} + \Delta R$, and on the t-axis $t_n = t_{n-1} + \Delta t$. Let W_j^n, w_j^n denote approximations to $W(R_j, z_0, t_n)$, $w(R_j, z_0, t_n)$, respectively. We also use the notation that on an R-coordinate line the coordinate z takes the constant value z_0.

Using the relationship $W(R_j, z_0, t_n) = Rw(R_j, z_0, t_n)$, we may write

$$W_j^n = \hat{R}w_j^n,$$ (2.9)

where $\hat{R}$ represents an average value of R. Assuming that at any time $t_n = n\Delta t$, W_j^n represents a piecewise constant approximation to $W(R_j, z_0, t_n)$ in the interval $(R_j - \Delta R/2, R_j + \Delta R/2)$ (as in the usual Godunov approach), $\hat{R}$ is given by the integral

$$\hat{R} = \frac{1}{\Delta R} \int_{R_j - \Delta R/2}^{R_j + \Delta R/2} R \, \mathrm{d}R = R_j,$$ (2.10)

i.e.

$$W_j^n = R_j w_j^n.$$ (2.11)

We can then recover the approximation w_j^n to $w(R_j, z_0, t_n)$ at time $t = t_n$ from equation (2.11), i.e.,

$$w_j^n = W_j^n / R_j. \qquad (2.12)$$

Consider the interval $[R_{j-1}, R_j]$ and denote by W_{j-1}, W_j the approximations to W at R_{j-1}, R_j, respectively. We now rewrite equation (2.7) as

$$W_t + \frac{\partial F(W)}{\partial W} W_R = r(w) \qquad (2.13)$$

and solve the associated one-dimensional Riemann problem

$$W_t + \tilde{A}(W_{j-1}, W_j)W_R = r(w) \qquad (2.14)$$

with data W_{j-1}, W_j at either side of the point $R_{j-1/2}$, linearising A in the form $\tilde{A}(W_{j-1}, W_j)$ which is then taken to be a constant matrix. We shall use the approximate form of equation (2.14),

$$\frac{W_j^{n+1} - W_j^n}{\Delta t} + \tilde{A}(W_{j-1}, W_j)\frac{(W_j - W_{j-1})}{\Delta R} = \tilde{r}(w^n) \qquad (2.15)$$

where $\tilde{A}(W_{j-1}, W_j)$ is the Roe matrix (2.17) (see [1]), $\tilde{r}$ is an approximation to r and J may be $j - 1$ or j. The Roe matrix $\tilde{A}(W_{j-1}, W_j)$ is an approximation to the Jacobian $A = \partial F(W)/\partial w$ and because of the remarks following equation (2.6e) it can be seen that

$$\tilde{A}(W_{j-1}, W_j) = \tilde{A}(w_{j-1}, w_j) \qquad (2.16)$$

where $\tilde{A}(w_{j-1}, w_j)$ is an approximation to $\partial f(w)/\partial w$. The Roe matrix is constructed so that

$$f_j - f_{j-1} = \tilde{A}(w_{j-1}, w_j)(w_j - w_{j-1})$$

for any finite change of state and is given [1] by

$$\tilde{A} = \begin{bmatrix} 0 & 1 & 0 & 0 \\ \dfrac{(\gamma - 1)}{2}\tilde{Q}^2 - \tilde{U}^2 & (3 - \gamma)\tilde{U} & -(\gamma - 1)\tilde{V} & \gamma - 1 \\ -\tilde{U}\tilde{V} & \tilde{V} & \tilde{U} & 0 \\ \dfrac{(\gamma - 1)}{2}\tilde{U}\tilde{Q}^2 - \tilde{U}\tilde{H} & \tilde{H} - (\gamma - 1)\tilde{U}^2 & -(\gamma - 1)\tilde{U}\tilde{V} & \gamma\tilde{U} \end{bmatrix} \qquad (2.7)$$

where $\tilde{Y}$ denotes a square-root mean of left and right states of Y, namely,

$$\tilde{Y} = \frac{\sqrt{\mathcal{R}_{j-1}}\,Y_{j-1} + \sqrt{\mathcal{R}_j}\,Y_j}{\sqrt{\mathcal{R}_{j-1}} + \sqrt{\mathcal{R}_j}} \qquad (2.18)$$

for all variables other than $\mathscr{R}$ and ϱ, and

$$\tilde{Q}^2 = \tilde{U}^2 + \tilde{V}^2. \tag{2.19}$$

In later analysis we shall also need mean values for $\mathscr{R}$ and ϱ, given by

$$\tilde{\mathscr{R}} = \sqrt{\mathscr{R}_{j-1}\mathscr{R}_j}, \quad \tilde{\varrho} = \sqrt{\varrho_{j-1}\varrho_j}. \tag{2.20}$$

The eigenvalues of $\tilde{A}$ are

$$\lambda_1^R = \tilde{U} + \tilde{a}, \quad \lambda_2^R = \tilde{U} - \tilde{a}, \quad \lambda_{3,4}^R = \tilde{U}, \tag{2.21}$$

with corresponding eigenvectors

$$\tilde{e}_1^R = (1, \tilde{U} + \tilde{a}, \tilde{V}, \tilde{H} + \tilde{U}\tilde{a})^T, \tag{2.22a}$$

$$\tilde{e}_2^R = (1, \tilde{U} - \tilde{a}, \tilde{V}, \tilde{H} - \tilde{U}\tilde{a})^T, \tag{2.22b}$$

$$\tilde{e}_3^R = (1, \tilde{U}, \tilde{V}, \tfrac{1}{2}\tilde{Q}^2)^T, \tag{2.22c}$$

$$\tilde{e}_4^R = (0, 0, \tilde{V}, \tilde{V}^2)^T,$$

where $\tilde{H}$ is calculated using equation (2.18), and the mean sound speed $\tilde{a}$ is calculated from

$$\tilde{a}^2 = (\gamma - 1)(\tilde{H} - \tfrac{1}{2}\tilde{Q}^2). \tag{2.23}$$

Using the above properties of $\tilde{A}$ we can write equation (2.14) as

$$\frac{W_j^{n+1} - W_j^n}{\Delta t} + \frac{F_j - F_{j-1}}{\Delta R} = \tilde{r}(w^n) \tag{2.24}$$

where $\tilde{r}(w^n)$ is a suitable approximation to the term $r(w)$ on the right-hand side of equation (2.14). We thus obtain

$$W_j^{n+1} - W_j^n = \Delta t\, \tilde{r}(w^n) - \frac{\Delta t}{\Delta R}(F_j - F_{j-1}). \tag{2.25}$$

In the Cartesian case the procedure [1] is to project $\Delta f = f_j - f_{j-1}$ onto the eigenvectors of $\tilde{A}$. Each projection represents the contribution of one wave system to Δf. Here we follow a suggestion of Roe [3] for the one-dimensional case of duct flow, and find projections both of $\Delta F = F_j - F_{j-1}$ and also $\tilde{r}(w^n)$. Specifically, we write

$$\Delta W = W_j - W_{j-1} = \sum_{i=1}^{4} \tilde{\alpha}_i^R \tilde{e}_i^R \tag{2.26}$$

so that

$$\Delta F = F_j - F_{j-1} = \sum_{i=1}^{4} \tilde{\lambda}_i^R \tilde{\alpha}_i^R \tilde{e}_i^R. \tag{2.27}$$

Since $\tilde{A}$ has eigenvalues $\tilde{\lambda}_i^R$ with corresponding eigenvectors $\tilde{e}_i^R$, and

$$\tilde{r}(w^n) = -\frac{1}{\Delta R} \sum_{i=1}^{4} \tilde{\beta}_i^R \tilde{e}_i^R \tag{2.28}$$

we may rewrite equations (2.25) as

$$W_j^{n+1} = W_j^n - \frac{\Delta t}{\Delta R} \sum_{i=1}^{4} \tilde{\lambda}_i^R \tilde{\gamma}_i^R \tilde{e}_i^R \tag{2.29}$$

where

$$\tilde{\gamma}_i^R = \tilde{\alpha}_i^R + \tilde{\beta}_i^R / \tilde{\lambda}_i^R$$

and J may be $j - 1$ or j.

A similar analysis follows for updating along a z-coordinate line, $R = R_0$. In that case equation (2.9) becomes

$$W_k^n = \hat{R} w_k^n \tag{2.31}$$

where W_k^n, w_k^n represent approximations to $W(R_0, z_k, t_n)$, $w(R_0, z_k, t_n)$, respectively, and

$$\hat{R} = \frac{1}{\Delta z} \int_{z_k - \Delta z/2}^{z_k + \Delta z/2} R_0 \, dz = R_0 \tag{2.32}$$

(Δz represents the mesh spacing in the z-direction). Moreover, since equation (2.8) has a zero right-hand side, the corresponding expression to equation (2.29) in this case is

$$W_K^{n+1} = W_K^n - \frac{\Delta t}{\Delta z} \sum_{i=1}^{4} \tilde{\lambda}_i^z \tilde{\alpha}_i^z \tilde{e}_i^z \tag{2.33}$$

where $\tilde{\lambda}_i^z$, $\tilde{e}_i^z$ take similar forms to those given by equations (2.21)–(2.22d) and $\tilde{\alpha}_i$ satisfy

$$G_k - G_{k-1} = \sum_{i=1}^{4} \tilde{\lambda}_i^z \tilde{\alpha}_i^z \tilde{e}_i^z. \tag{2.34}$$

To update W^n to W^{n+1} we apply a sequence of one-dimensional calculations along computational grid lines in the R and z directions in turn. The algorithm along any coordinate line uses first-order upwind differencing. In particular, along an R-coordinate line we add $-(\Delta t/\Delta R)\tilde{\lambda}_i^R \tilde{\gamma}_i^R \tilde{e}_i^R$ to W_j^n when $\tilde{\lambda}_i^R > 0$ or add $-(\Delta t/\Delta R)\tilde{\lambda}_i^R \tilde{\gamma}_i^R \tilde{e}_i^R$ to W_{j-1}^n when

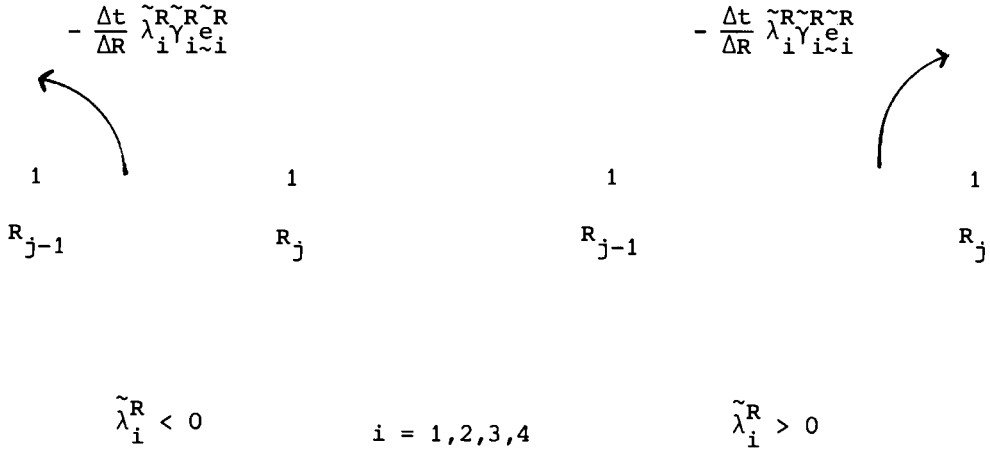$$- \frac{\Delta t}{\Delta R} \tilde{\lambda}_i^R \tilde{\gamma}_i^R \tilde{e}_{\sim i}^R$$

1

R_{j-1}

1

R_j

$$- \frac{\Delta t}{\Delta R} \tilde{\lambda}_i^R \tilde{\gamma}_i^R \tilde{e}_{\sim i}^R$$

1

R_{j-1}

1

R_j

$$\tilde{\lambda}_i^R < 0 \qquad i = 1,2,3,4 \qquad \tilde{\lambda}_i^R > 0$$

Fig. 1(a). Schematic representation of the first-order algorithm in the *R*-direction.

$$- \frac{\Delta t}{\Delta z} \tilde{\lambda}_i^z \tilde{\alpha}_i^z \tilde{e}_{\sim i}^z$$

1

z_{j-1}

1

z_j

1

z_{j-1}

$$- \frac{\Delta t}{\Delta z} \tilde{\lambda}_i^z \tilde{\alpha}_i^z \tilde{e}_{\sim i}^z$$

1

z_j

$$\tilde{\lambda}_i^z < 0 \qquad\qquad \tilde{\lambda}_i^z > 0$$
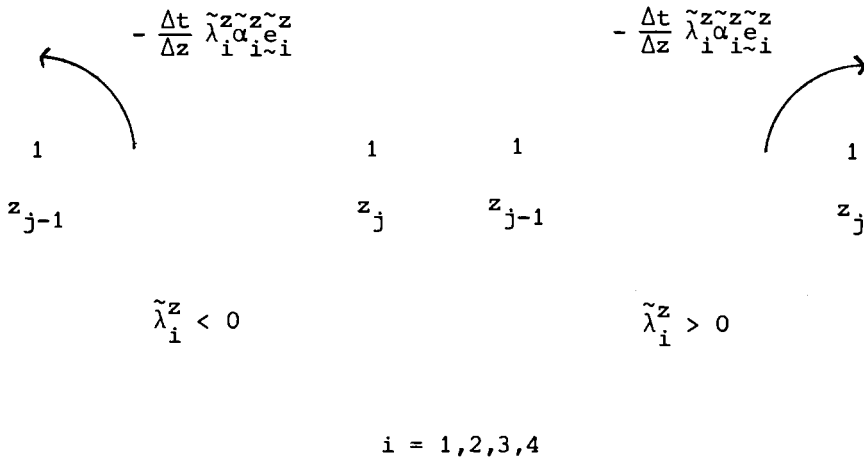
$$i = 1,2,3,4$$

Fig. 1(b). Schematic representation of the first-order algorithm in the *z*-direction.

$\tilde{\lambda}_i^R < 0$ for each cell $[R_{j-1}, R_j]$ (see Fig. 1(a)). A similar procedure is implemented along a *z*-coordinate line (see Fig. 1(b)).

If we follow through the algebra, we obtain the following expressions for $\tilde{\alpha}_i^R$, $\tilde{\beta}_i^R$ in equation (2.29):

$$\tilde{\alpha}_1^R = \frac{1}{2\bar{a}^2} (\Delta P + \tilde{\mathcal{R}} \bar{a} \Delta U), \tag{2.35a}$$

$$\tilde{\alpha}_2^R = \frac{1}{2\bar{a}^2} (\Delta P - \tilde{\mathcal{R}} \bar{a} \Delta U), \tag{2.35b}$$

$$\tilde{\alpha}_3^R = \Delta \mathcal{R} - \frac{\Delta P}{\bar{a}^2}, \tag{2.35c}$$

$$\tilde{\alpha}_4^R = \frac{\tilde{\mathscr{R}}}{\tilde{V}} \Delta V, \tag{2.35d}$$

$$\tilde{\beta}_1^R = \frac{\Delta R \hat{r}_2}{2\tilde{a}^2} (\tilde{a} + (\gamma - 1)\tilde{U}), \tag{2.36a}$$

$$\tilde{\beta}_2^R = -\frac{\Delta R \hat{r}_2}{2\tilde{a}^2} (\tilde{a} - (\gamma - 1)\tilde{U}), \tag{2.36b}$$

$$\tilde{\beta}_3^R = -\frac{\Delta R \hat{r}_2}{\tilde{a}^2} (\gamma - 1)\tilde{U}, \tag{2.36c}$$

$$\tilde{\beta}_4^R = 0, \tag{2.36d}$$

where $\Delta(\cdot) = (\cdot)_j - (\cdot)_{j-1}$. Similar expressions hold for $\tilde{\alpha}_i^z$, and we have already noted that $\tilde{\beta}_i^z = 0$. The coefficients $\tilde{\beta}_i^R$ have been determined by setting

$$-\frac{1}{\Delta R} \sum_{i=1}^{4} \tilde{\beta}_i^R \tilde{e}_i^R = \begin{pmatrix} 0 \\ \hat{r}_2 \\ 0 \\ 0 \end{pmatrix}, \tag{2.37}$$

and choosing a suitable approximation $\hat{r}_2$ to the term $r_2 = p \, \partial(R)/\partial R$ of equation (2.6d). We write $r_2 = (\varrho a^2/\gamma) \, \partial(R)/\partial R$ and approximate

$$\hat{r}_2 = \frac{\tilde{\varrho}\tilde{a}^2}{\gamma} \frac{\Delta(R)}{\Delta R} = \frac{\tilde{\varrho}\tilde{a}^2}{\gamma}, \tag{2.38}$$

where $\tilde{\varrho} = \sqrt{\varrho_{j-1}\varrho_j}$ as in the Cartesian case. Finally, we note that

$$\tilde{\varrho} = \sqrt{\varrho_{j-1}\varrho_j} = \sqrt{\frac{\mathscr{R}_{j-1}}{\hat{\mathscr{R}}_{j-1}} \frac{\mathscr{R}_j}{\hat{\mathscr{R}}_j}} = \frac{\tilde{\mathscr{R}}}{\tilde{R}} \tag{2.39}$$

where $\tilde{R} = \sqrt{\hat{R}_{j-1}\hat{R}_j} = \sqrt{R_{j-1}R_j}$ is averaged in the same way as ϱ, $\mathscr{R}$. Therefore

$$\hat{r}_2 = \frac{\tilde{\mathscr{R}}\tilde{a}^2}{\tilde{R}\gamma} \tag{2.40}$$

and $\tilde{\beta}_i^R$ are given by

$$\tilde{\beta}_1^R = \frac{\tilde{\mathscr{R}}\Delta R}{2\gamma\tilde{R}} (\tilde{a} + (\gamma - 1)\tilde{U}), \tag{2.41a}$$

$$\tilde{\beta}_2^R = -\frac{\tilde{\mathscr{R}}\Delta R}{2\gamma\tilde{R}} (\tilde{a} - (\gamma - 1)\tilde{U}), \tag{2.41b}$$

$$\tilde{\beta}_3^R = -\frac{\tilde{\mathcal{R}}\Delta R}{\gamma \tilde{R}}(\gamma - 1)\tilde{U},\tag{2.41c}$$

$$\tilde{\beta}_4^R = 0.\tag{2.41d}$$

Summarising, we project the initial data $w(R, z, 0)$ onto a set of piecewise-constant states $W_{jk}^0 = R_j w(R_j, z_k, 0)$ on the rectangle

$$(R_j - \Delta R/2, R_j + \Delta R/2) \times (z_k - \Delta z/2, z_k + \Delta z/2),$$

march forward to a time $m\Delta t$ using a time step Δt by sweeping m times in the R- and z-directions alternatively as described by equations (2.18)–(2.41d), and recover the approximate solution using

$$w_{jk}^{m\Delta t} = W_{jk}^{m\Delta t}/R_j.$$

In addition to the first-order algorithm given here, we can calculate second-order corrections by transferring fractions of the increments described in Figs. 1(a)–(b) (see [4–6]). If we limit these transfers using a suitable flux limiter or B-function (see [4–6]), the scalar scheme will be second-order almost everywhere, oscillation-free, and will sharpen up certain features that would be smeared by using the first-order method only.

In the next section we describe a test problem that can be used to test the algorithm of this section.

3. Numerical results

In this section we describe a test problem that can be used to test the algorithm of Sec. 2 and display the numerical results obtained.

This two-dimensional shock tube problem can be considered either in (x, y) or (R, z) geometry (see Glaister [7]).

Consider the two-dimensional Euler equations with axial symmetry and the region $(R, z) \in [0, 1] \times [0, 1]$ with rigid boundaries along $R = 0, z = 0$. We position a membrane along (R, z) where $\sqrt{R^2 + z^2} = \frac{1}{2}$ and take initial data

$$(\varrho, u, v, p) = \begin{cases} (\varrho_-, 0, 0, p_-) & \text{if} \quad \sqrt{R^2 + z^2} < \frac{1}{2}, \\ (\varrho_+, 0, 0, p_+) & \text{if} \quad \sqrt{R^2 + z^2} > \frac{1}{2}. \end{cases}$$

The solution to this problem has spherical symmetry and satisfies the corresponding "one-dimensional" Euler equations (see Ref. [7]). Thus we can see whether the solution remains symmetric: moreover, we can compare the results with those obtained using a "one-dimensional" algorithm for the Euler equations with spherical symmetry.

Figures 2–5 refer to this problem and the two-dimensional results have been computed using the algorithm of Sec. 2. We have taken $\gamma = 1.4$, a mesh with 50×50 grid points and a time step $\Delta t = 0.004$. For each output time we draw 31 equally spaced contours at

A Converging Spherical Shock

1-d solution with 800 points

1-d solution with 50 points

2-d solution along R=z
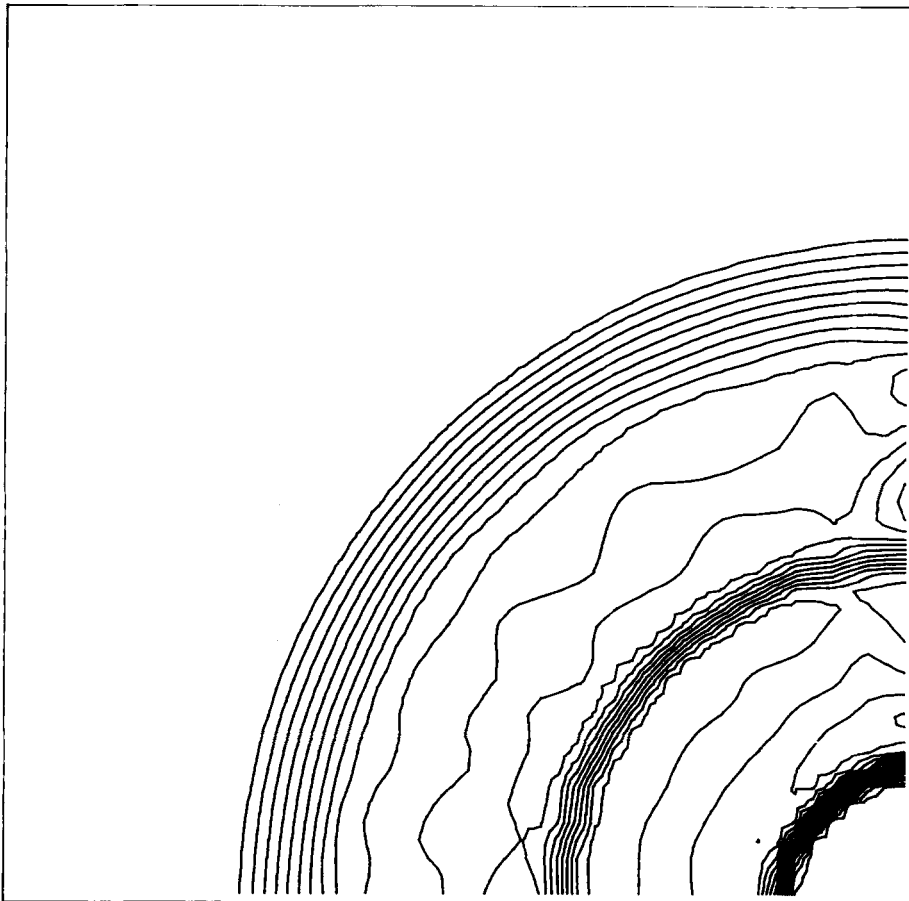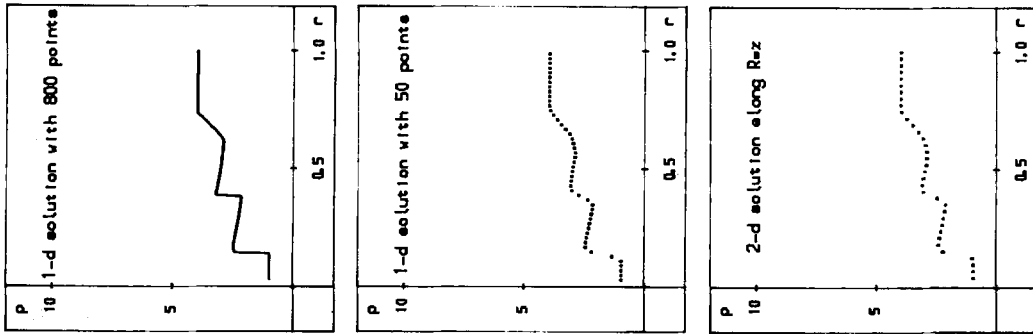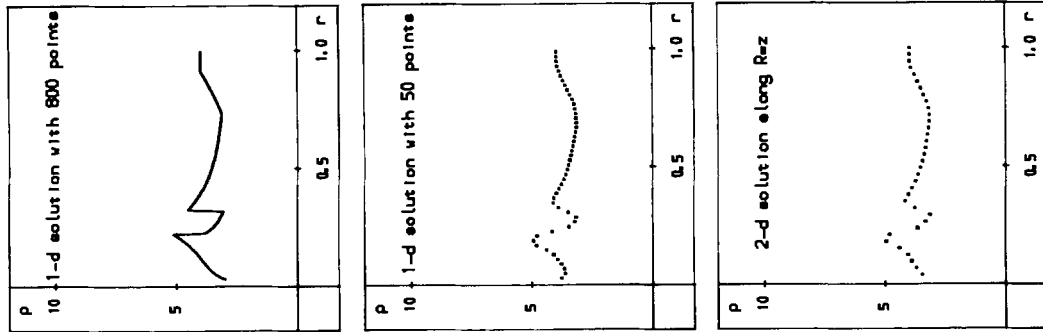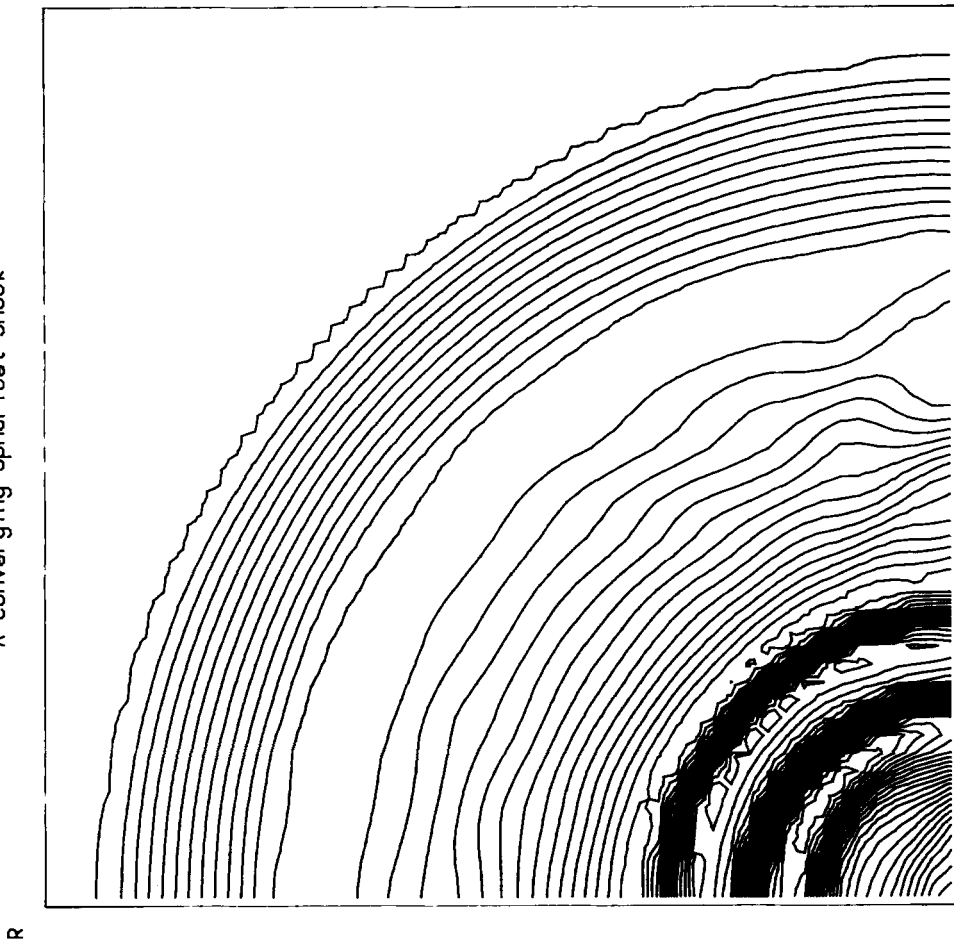
Density at t = 0.200 , contours from 1.000 to 4.000

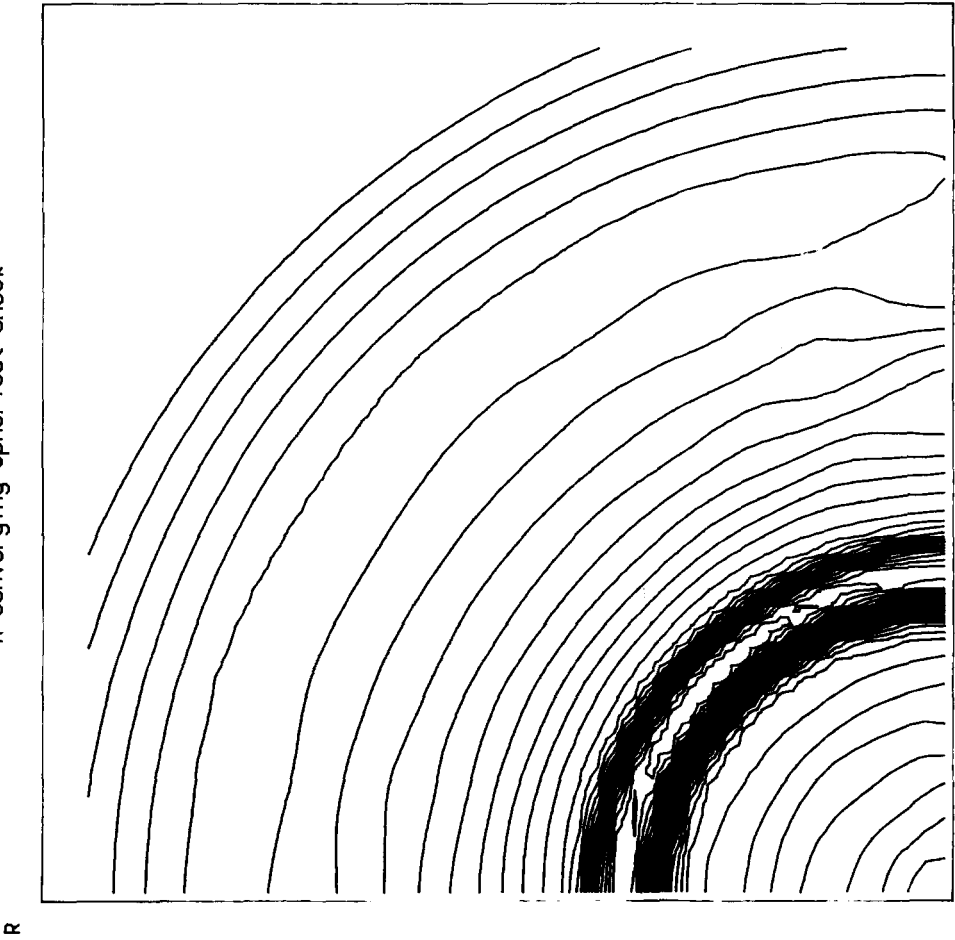*Fig. 2.* Results for the problem of Sec. 3 at $t = 0.200$. The converging shock approaches $R = z = 0$.

Density at t = 0.352 , contours from 3.164 to 5.012

Fig. 3. Results for the problem of Sec. 3 at $t = 0.352$. The shock, having been reflected from $R = z = 0$, is headed towards the converging contact discontinuity.

A Converging Spherical Shock
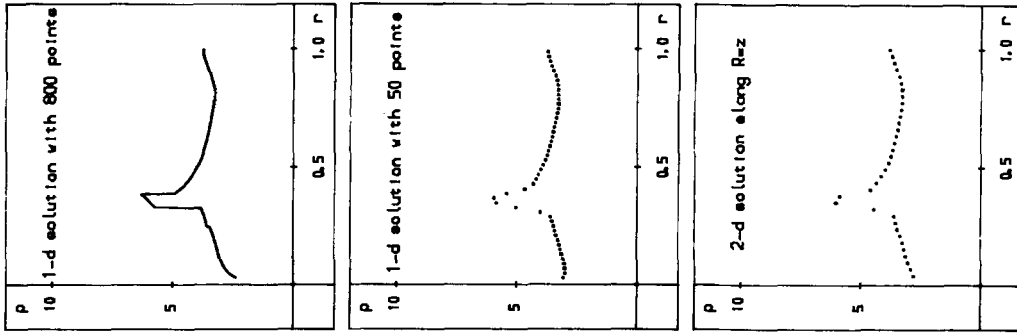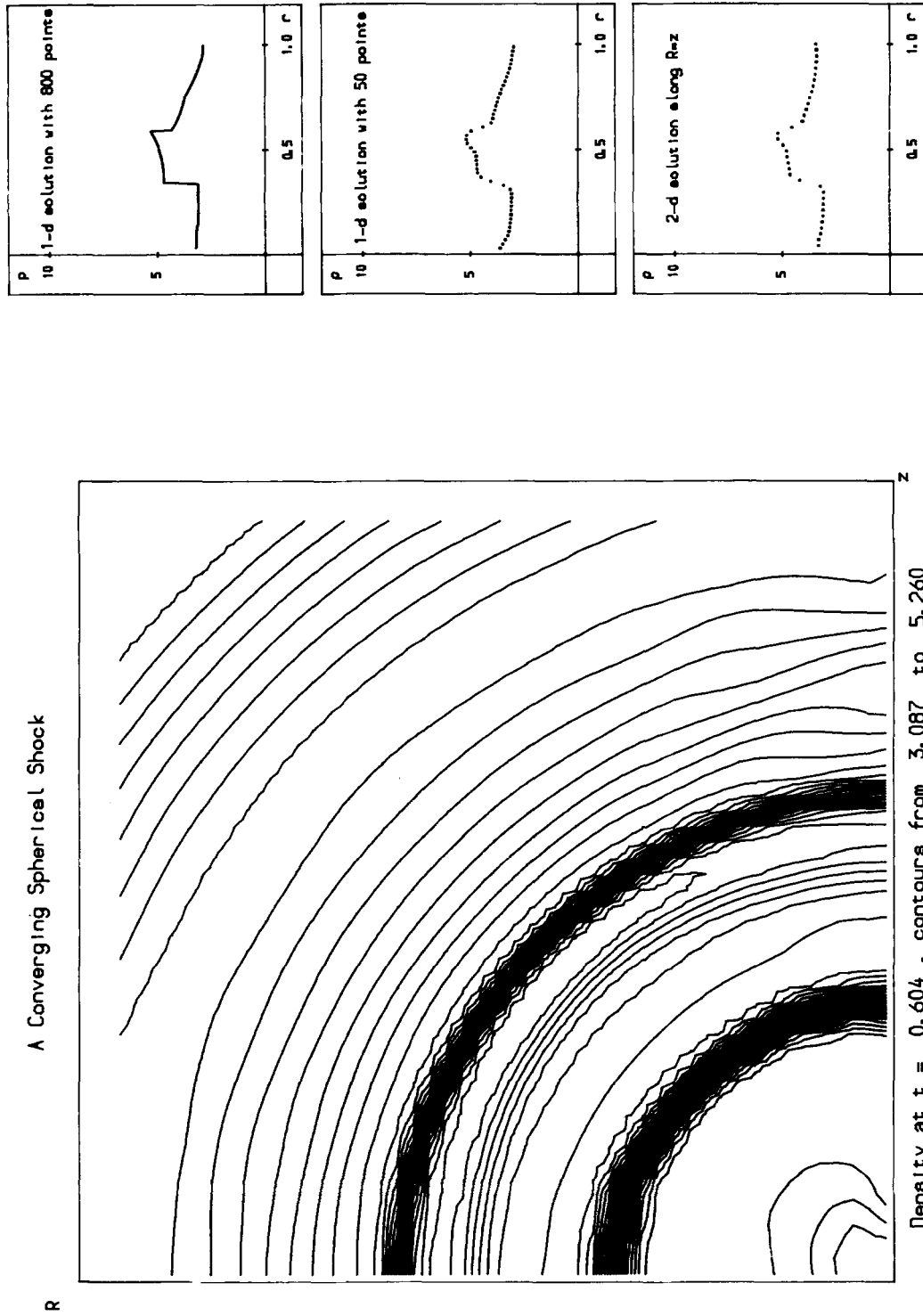
Density at t = 0.452 , contours from 2.766 to 6.104

Fig. 4. Results for the problem of Sec. 3 at $t = 0.452$. The interaction of the shock and contact discontinuity.

Density at t = 0.604, contours from 3.087 to 5.260

Fig. 5. Results for the problem of Sec. 3 at *t* = 0.604. The interaction results in a diverging transmitted shock, a converging contact discontinuity and a weak converging shock.

$\varrho_{min} + (i/30)(\varrho_{max} - \varrho_{min}), i = 0, 1, \ldots 30$, where $\varrho_{min}, \varrho_{max}$ are the minimum and maximum densities throughout the flow, respectively. In addition, we plot the density along $R = z$ and plot the solution to the corresponding one-dimensional spherical problem obtained using the algorithm of Glaister [2] with 50 and 800 points. The one-dimensional solution with 800 points provides a good approximation to the exact solution, whereas the solution with 50 points provides a comparison on similar grids.

The initial discontinuity breaks up into a converging shock and contact discontinuity. The shock is reflected from $R = z = 0$ and interacts with the contact discontinuity. This results in a transmitted shock together with the contact discontinuity still converging. These features are apparent in Figs. 2, 3, 4, 5, respectively. For each figure we see that the two-dimensional solution obtained remains symmetrical and is comparable to the one-dimensional solution on a similar grid. Furthermore, the solution clearly models the high resolution obtained with 800 points. All computations have been done using the second-order entropy satisfying scheme with the "superbee" limiter (see [6]).

The c.p.u. time used to compute these results using an Amdahl V7 with a 50 × 50 mesh is as follows. The algorithm takes 1.2 c.p.u. seconds to compute one time step and 60 c.p.u. seconds to reach a real time of 0.2 using 50 time steps.

Along the walls $R = 0, z = 0$ we apply reflecting boundary conditions. Specifically, along $z = 0$, we consider an image cell and impose equal density, pressure and tangential velocity (u in this case), and equal and opposite normal velocity (v in this case), at either end of the cell. A similar argument applies for a reflecting boundary condition along $R = 0$.

4. Conclusions

We have proposed an algorithm for the Euler equations with axial symmetry which is an extension of the schemes of Roe [1] and Glaister [2], and incorporates the technique of operator splitting. The algorithm has been applied to the test problem of a converging spherical shock and has achieved satisfactory results.

Acknowledgements

References

1. P.L. Roe, Approximate Riemann solvers, parameter vectors, and difference schemes, *J. Comput. Phys.* 43 (1981) 357–372.
2. P. Glaister, Flux difference splitting for the Euler equations in non-Cartesian geometry, *Numerical Analysis Report* 8–85, University of Reading (1985).
3. P.L. Roe, Upwind differencing schemes, hyperbolic conservation laws with source terms, *1st Int. Congress on Hyperbolic Problems*, St. Etienne (1986), (ed. C. Carassa, D. Serre), (to appear).
4. P.L. Roe, Some contributions to the modelling of discontinuous flows, *Proc. AMS/SIAM Seminar*, San Diego (1983).

5. P.L. Roe and J. Pike, Efficient construction and utilisation of approximate Riemann solutions, *Computing Methods in Applied Science and Engineering* VI (1984) 499–518.

6. P.K. Sweby, High resolution schemes using flux limiters for hyperbolic conservation laws, *SIAM J. Numer. Anal.* 21 (1984) 995–1011.

7. P. Glaister, Similarity solutions for shock reflection problems in gas dynamics, *Numerical Analysis Report* 13–86, University of Reading (1986).